International Journal of Innovative
Computing, Information and Control
Volume **19**, Number **3**, June **2023**

ICIC International ©2023 ISSN 1349-4198
pp. 699–719

OPTIMIZATION OF TORSIONAL STIFFNESS FOR OPERATIONAL EASINESS OF LARGE TOWER CRANES BY MINIMIZING VIBRATION GAINS

Hideki Takahashi[1,2], Fumiya Tsukahara[1], Kenichi Terauchi[2]
Shintaro Sasai[2], Hitoshi Sakurai[2], Masaki Okubo[2] and Naoki Uchiyama[1,*]

[1]Department of Mechanical Engineering
Toyohashi University of Technology
1-1, Hibarigaoka, Tempaku, Toyohashi 441-8580, Japan
{ takahashi.hideki.xq; tsukahara.fumiya.ka }@tut.jp
*Corresponding author: uchiyama@tut.jp

[2]Kobelco Construction Machinery Co., Ltd.
740, Okubo, Akashi 674-0063, Japan
{ terauchi.kenichi; sasai.shintaro; sakurai.hitoshi; okubo.masaki }@kobelco.com

Received October 2022; revised January 2023

Abstract. *In manufacturing industry of large cranes, the operational easiness is crucial due to being shortage of skilled operators. Large cranes are being made lighter to improve their transportability. However, a reduction in the rigidity of a tower due to the light weight of its components makes the tower boom more prone to vibration due to torsional elastic deformation, reducing the operability of the crane. In this study, the torsional stiffness of the tower, the rope length, and the mass of load were varied to analyze the effect of vibration due to tower elasticity on the operator's load-sway suppression. The torsional stiffness required to improve the operability was determined using the average, variance, and maximum of the signal amplification gains at the secondary vibration frequency. Additionally, an experimental crane was designed to confirm the validity of the obtained analytical results. Human operators performed manipulation experiments, and statistical evaluations were used to confirm that the proposed optimum torsional stiffness was effective in improving the operability.*

Keywords: Large tower crane, Tower boom stiffness, Optimization, Load-sway suppression, Crane operability

1. **Introduction.** Large cranes are widely used to handle heavy loads by skilled operators at various construction sites because of their versatility. Hence, the maintenance and operation easiness is important in their design and manufacturing due to being shortage of skilled workers [1]. A large crane consists of a lower traveling body, upper slewing body, counterweight, gantry, tower boom (hereinafter called "tower"), and jib (Figure 1). Large cranes are increasing in size to meet high capacity demands, and some cranes with maximum lifting capacities exceeding 1,000 tons are in use. Generally, large cranes are transported in components and are disassembled and assembled at the site where they will be used. The maximum loading weight limit for trailers in Japan is lower than that in other countries; therefore, weight reduction in components must improve transportability [2, 3, 4, 5]. Elastic vibration will be a problem in the operation because there is a trade-off between weight reduction and attachment (i.e., jib and tower) rigidity. Large crane attachments are made of trusses with high compressive stiffness but low torsional stiffness. Because the jib is connected to the tower in a horizontal position, tower

DOI: 10.24507/ijicic.19.03.699

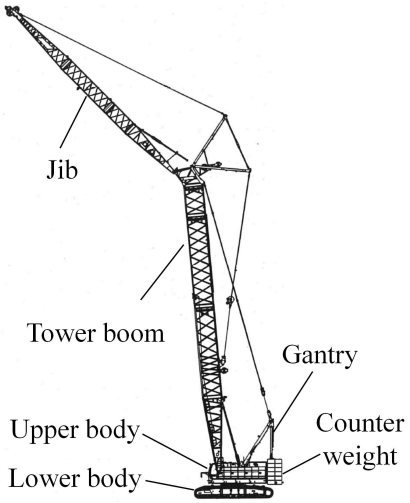

FIGURE 1. Schematic of a tower crane

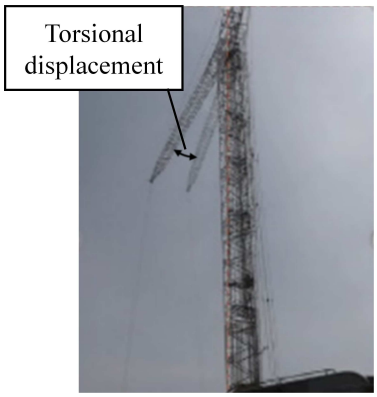

FIGURE 2. Torsional displacement of a tower

torsion occurs (Figure 2). If the load-sway contains a tower vibration mode (hereafter the "second-order mode" because the first mode corresponds to the load-rope system), load-sway suppression by operators becomes difficult. Additionally, from the operator's room, the operator can see only the load-sway, not the jib-sway, making it difficult to suppress the load-sway. Therefore, it is desirable to synchronize load-sway and tower torsion by design. In other words, a design that reduces the second-order vibration mode is required. There exist mechanical design approaches to vibration suppression by considering the stiffness. For example, Zhou et al. proposed to suppress mechanical vibration in a wind power generation system by using the stiffness of the transmission chain [6]. Wu et al. suppressed the lateral vibration of a steel rope by changing the stiffness of a guide shoe in a high-speed elevator [7]. In this paper, a design method of torsional stiffness of towers for operational easiness considering load-sway suppression is investigated. Many studies have been conducted on software approaches to load-sway suppression for cranes; for example, load-sway reduction by feedforward control [8, 9, 10, 11], feedback control [12, 13, 14, 15, 16], and controller design combining them, optimal control of load-sway and load handling time using a linear transfer model [17], control based on linear matrix inequality optimization for robustness against rope length variation [18], control to provide the robustness to disturbances [19], high-performance nonlinear control to track specified load-sway suspension trajectory [20], load-sway suppression considering the torsional stiffness of the tower [21], nonlinear control without velocity feedback [22], adaptive

nonlinear control [23], energy-shaping-based nonlinear control [24], and open-loop control by only horizontal boom motion [25]. However, for large cranes, implementations of these automatic controllers are still difficult because of issues on safety including emergency stop functions, sensor installation and actuator hydraulic properties [26, 27, 28]. Hence, this study focuses on the improvement of manual operation easiness by hardware design optimization. The instability caused by attachment stiffness has also been studied. Azeloglu et al. [29] confirmed that the finite element analysis of a scaled physical model of a lattice structure boom can yield a more accurate frequency response of the crane. Kong et al. [30] used the co-rotating finite element method to analyze the geometric nonlinear elastic instability of a lattice boom structure and confirmed that the unstable load of a tower crane boom can be observed by monitoring the derivative of the displacement and the sudden change in the singularity of the tangential stiffness matrix. Many studies have been conducted to suppress load-sway through software, but few studies have been conducted to suppress it through mechanical design. In this study, we focus on the torsional rigidity of a tower and consider a torsional rigidity design method that makes it easy to suppress residual load-sway. Load-sway motion is divided into two directions; radial and tangential sway to boom rotational circular direction. In most studies, the radial load-sway is controlled by the jib hoisting and lowering the motion, and the tangential direction by the boom rotational motion [31, 32]. Load-sway in the radial direction is small because large cranes are transported at low speeds for safety reasons. This study considers only the tangential load-sway.

In this study, we propose a method for optimizing the operability of a crane by reducing second-order mode vibration, which varies with the rope length and load mass, and we verify the effectiveness of the method through experiments. The dynamic model of the crane that was used in the simulation considering tower torsion is described in Section 2. The optimization of the tower torsional stiffness to improve the operability is described in Section 3. An experimental system with an elastic joint added to the main body to evaluate the operability of the designed torsional stiffness is described in Section 4. Section 5 presents the results of human manipulation experiments and discusses the effectiveness of the optimization. Finally, Section 6 concludes the study.

2. Dynamic Model of Crane Considering Tower Torsion.

2.1. Actual crane motion characteristics.

This section presents the characteristics of a commercial crane and discusses the effects of stiffness based on jib behavior and load-sway due to tower torsion. Table 1 shows the crane parameter values, and the attachment posture of the commercial tower crane (Kobelco Construction Machinery 7120G-2) whose behavior was measured as shown in Figure 3.

Figure 4 shows an example of the behavior of a commercial tower crane. The rotation speed ω in the tower changes in the following order: gradual acceleration, constant

Table 1. Parameter values of the tower crane in Figure 3

Item	Symbol [Unit]	Value
Tower length	L_t [m]	51.7
Jib length	L_j [m]	44.2
Rope length	l [m]	64.8
Tower undulation angle	θ_t [deg]	89
Jib undulation angle	θ_j [deg]	20
Load mass	m [ton]	2.8

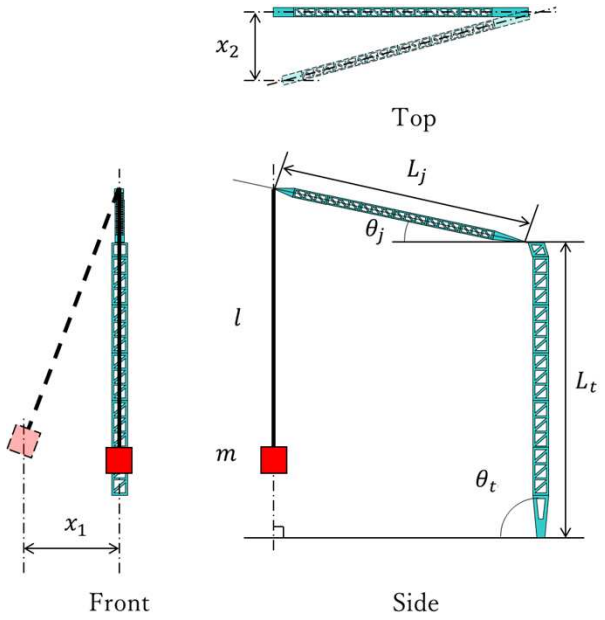

FIGURE 3. Displacement of a tower and a rope

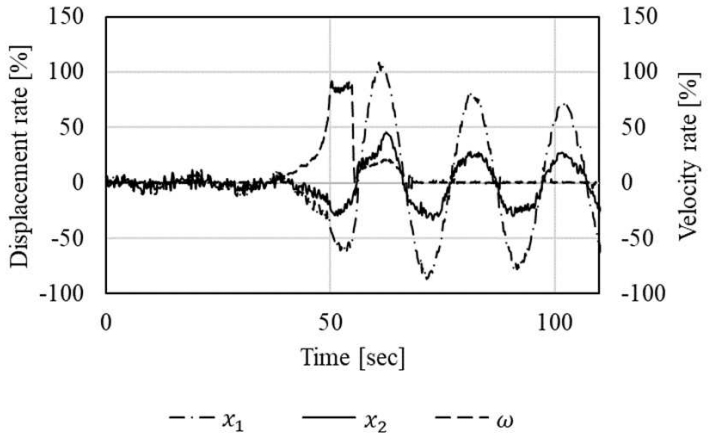

FIGURE 4. Load-sway and tower torsion of a tower crane

speed, and rapid deceleration. The load-sway (displacement x_1), and the tower torsion (displacement x_2) are shown in the figure. Displacements and angular velocity ω were normalized.

The tower is designed such that the tower torsion is synchronized with the load-sway based on the measurement results of commercial tower crane behavior. If the load-sway is not synchronized with the tower torsion, crane operation becomes difficult for operators.

2.2. **Liner dynamics model.** The nonlinear dynamics model used in [21] (hereinafter the "nonlinear model") was used in the simulation. Figure 5 compares the results of the nonlinear model with the behavior of the commercial crane when rotational angular velocity ω is given (Figure 4). The results agree well with each other (Figure 5), confirming the effectiveness of the nonlinear model. Load-sway in the radial direction is small because large cranes are transported at low speeds for safety reasons. Therefore, the dynamics model used in the following analysis does not consider the radial direction, but only the load-sway in the rotational direction as well as the tower torsion.

$$\dot{x} = \begin{bmatrix} 0 & 0 & 1 & 0 \\ 0 & 0 & 0 & 1 \\ \dfrac{-I_b g}{I_d} & \dfrac{lK}{I_d} & 0 & 0 \\ \dfrac{mlL_i g}{I_d} & -\dfrac{lK}{I_d} & 0 & 0 \end{bmatrix} x + \begin{bmatrix} 0 \\ 0 \\ -\dfrac{L_j K}{I_d} \\ \dfrac{lK}{I_d} \end{bmatrix} u \tag{1}$$

$$x = \begin{pmatrix} \theta_1, & \theta_2, & \dot{\theta}_1, & \dot{\theta}_2 \end{pmatrix}^T \tag{2}$$

$$I_b = \frac{1}{3}(m_t + m_j)L_j^2 + mL_j^2 \tag{3}$$

$$I_d = I_b L - mL_j^2 \tag{4}$$

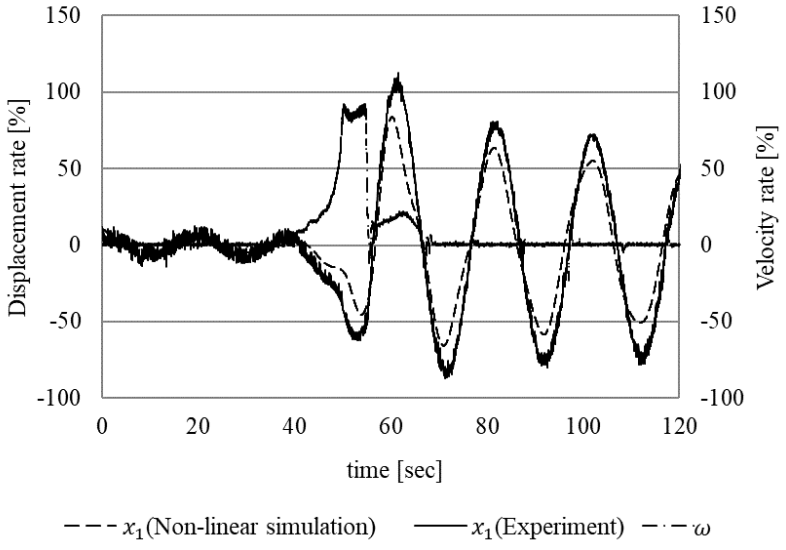

(a)

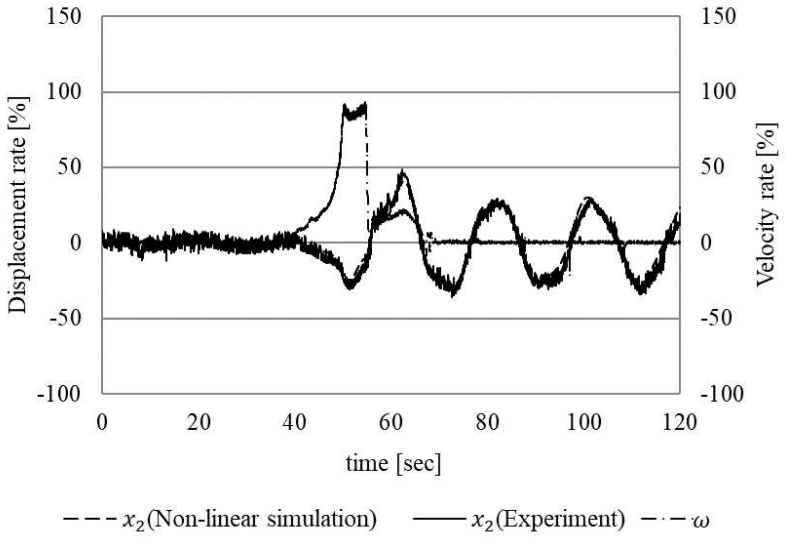

(b)

FIGURE 5. Comparison of actual crane and simulation results: (a) Load-sway angle and (b) tower torsional angle

Figure 6 shows a crane model with tower torsion whose linear dynamics are given in Equation (1), where notations and parameters values are shown in Table 2. Figure 7 compares the results of the analysis using the linear and nonlinear models with the behavior of a commercial crane. The linear model agrees well with the behavior of the actual one, confirming its validity.

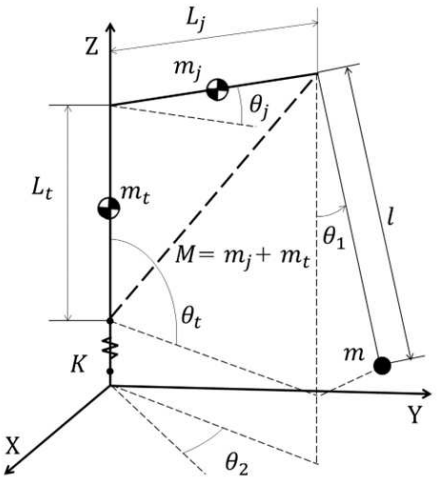

FIGURE 6. Crane model with load-sway and tower torsion

TABLE 2. Notations and values in the dynamics model in Equation (1) and Figure 6

Item	Symbol [Unit]	Value
Load-sway angle	θ_1 [deg]	–
Tower torsional angle	θ_2 [deg]	–
Angle and angular velocity vector	x [rad, rad/s]	–
Input actuator angle	u [rad]	–
Total inertia (Tower and Jib)	I_b [kgm^2]	–
Inertial parameter	I_d [kgm^3]	–
Tower mass	m_t [ton]	12.8
Jib mass	m_j [ton]	3.8
Load mass	m [ton]	2.8
Rope length	l [m]	56.4
Tower length	L_t [m]	51.7
Jib length	L_j [m]	44.2
Tower undulation angle	θ_t [deg]	89
Jib undulation angle	θ_j [deg]	20
Elastic constant	K [kNm/rad]	3000
Gravitational acceleration	g [m/s^2]	9.8

3. **Optimization of Tower Torsional Stiffness for Improved Operability.** As described in Section 1, when the load-sway and tower torsion are not synchronized, it is extremely difficult to perform anti-sway operations in large cranes because the crane operator cannot see the tower torsion but only the load-sway. Therefore, in the design, the signal amplification gains of the second-order mode corresponding to tower torsional vibration must be reduced. For example, when the torsional stiffness $K = 2.6 \times 10^3$ [kNm/

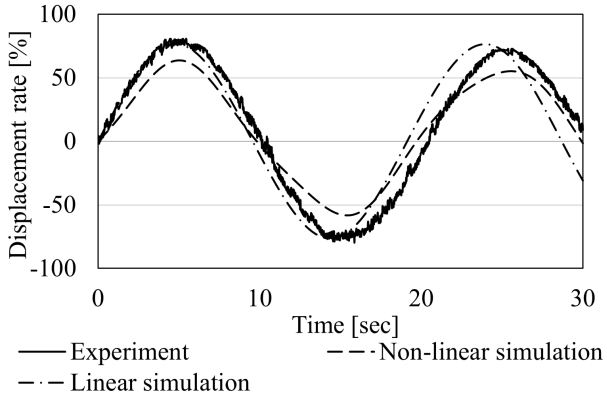

(a)

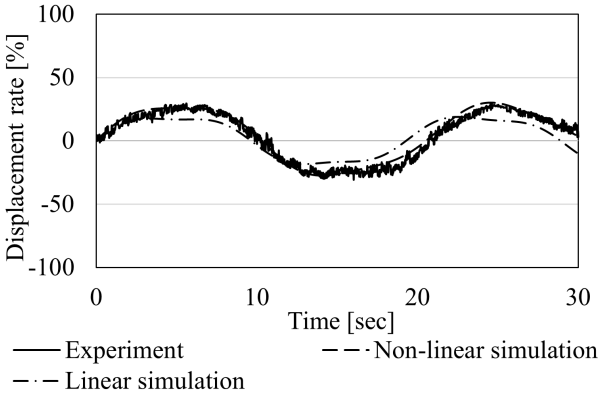

(b)

FIGURE 7. Comparison of actual crane and simulation results: (a) Load-sway angle and (b) torsional angle

rad] in Equation (1), the second-order mode is prominent (Figure 8(a)). However, it can be reduced when $K = 2.6$ [kNm/rad] (Figure 8(b)), enabling the operator to control load-sway.

The second-order mode gain depends not only on K but also on rope length l and load mass m, both of which may be changed at the work site. Therefore, it is desirable to achieve a robust optimization design that suppresses the second-order mode gain as much as possible for varying l and m. Example of calculation results of the second-order mode gain for a laboratory small crane, which is explained in detail later in Section 4, are shown in Figure 9. A total of 171 conditions, in which l is varied from 1.5 to 3 [m] in 0.1 [m] increments, and m is varied from 1 to 3 [kg] in 0.2 [kg] increments, are applied to Equation (1). These calculations were performed in 46 different conditions with K ranging from 10 to 250 [Nm/rad] in increments of 10 [Nm/rad].

As mentioned above, the second-order mode gain should be minimized to improve the operability. Here, we consider the following three gain minimization problems:

$$K_{ave} = \underset{K}{\text{argmin}} G_{ave}(K, l, m) \tag{5}$$

$$K_{var} = \underset{K}{\text{argmin}} G_{var}(K, l, m) \tag{6}$$

$$K_{\max} = \underset{K}{\text{argmin}} G_{\max}(K, l, m) \tag{7}$$

where G_{ave}, G_{var} and $G_{\max}$ are the average, variance and maximum of second-order mode gains over considered rope length and load mass, and K_{ave}, K_{var} and $K_{\max}$ are obtained torsional stiffness by minimization, respectively under dynamics Equation (1). The second-mode frequency can be obtained by applying parameter values l and m to the state matrix in Equation (1) and find its eigenvalues. Because Equation (1) does not include the viscous friction, the eigenvalues are conjugate imaginary ones, and eigenvalues with larger magnitudes correspond to the square of the second-mode angular frequency. Using this angular frequency, we can calculate the corresponding gain of the linear system in Equation (1). By changing l and m for all the defined region, we can calculate the average, maximum and variance of the gain of the linear system in Equation (1) numerically. By using these average, maximum and variance of the gain as objective functions, we can solve Equations (2)-(4) by nonlinear programming techniques such as the sequential quadratic programming.

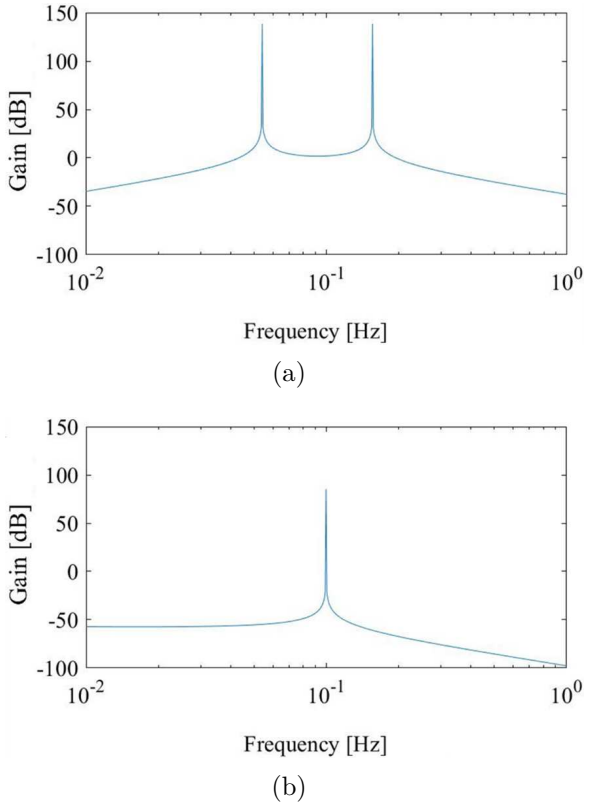

FIGURE 8. Elimination of the second-order mode by changing the torsional stiffness: (a) $K = 2.6 \times 10^3$ [kNm/rad] and (b) $K = 2.6$ [kNm/rad]

Here we not only calculate the minimum value, but also plot the gain diagram as shown in Figure 10 to see the relationship of the obtained minimum values. Figure 10 shows (a) the average, (b) variance, and (c) maximum of the second-order mode gains, where $L_t = 2.2$ [m], $L_j = 2.0$ [m], $m_t = 36$ [kg] and $m_j = 3.2$ [kg] are used considering the experiment in Section 4. Three optimal candidates of torsional stiffness $K = 10$, 110, and 200 [Nm/rad] were selected.

4. **Experimental System.**

4.1. **Design of an experimental crane considering tower torsion.**

Because a commercial crane is huge, with a rope length of approximately 55 [m], an experimental system

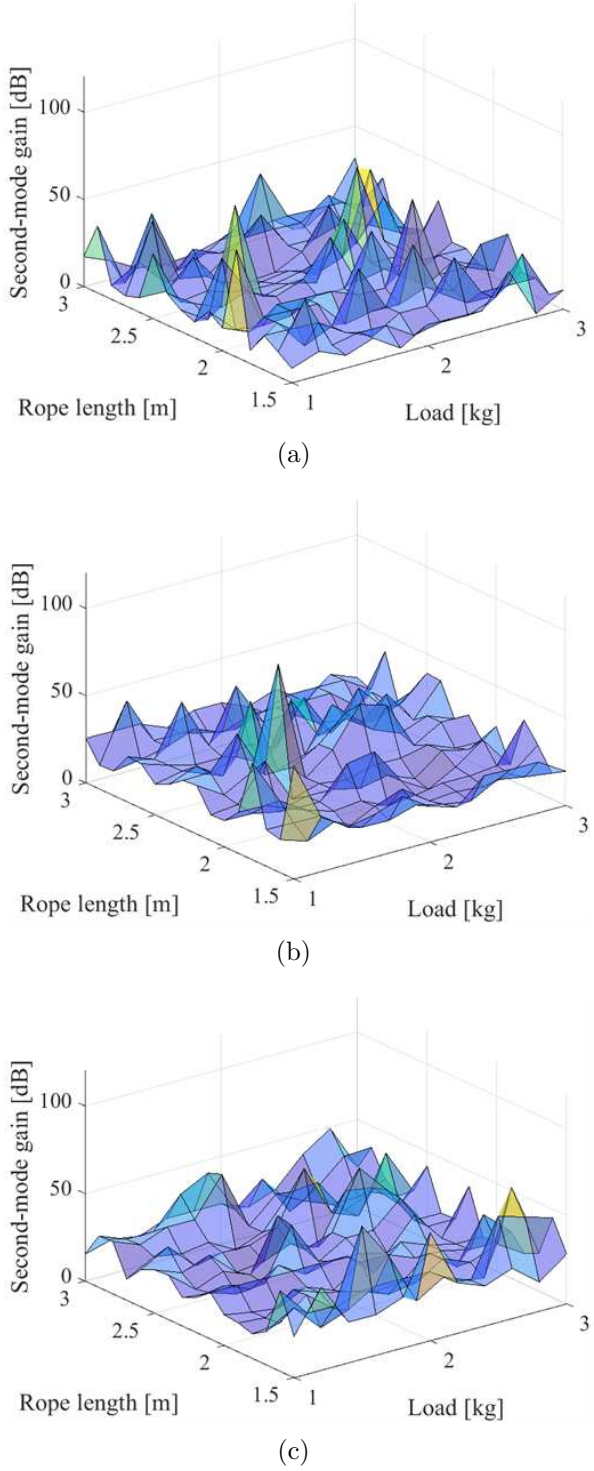

FIGURE 9. Simulation results of gains for the second-order mode: (a) $K = 10$ [Nm/rad], (b) $K = 100$ [Nm/rad] and (c) $K = 250$ [Nm/rad]

(hereinafter a "small crane") was designed with torsional rigidity for a safe experiment. The small crane is 1/21 scale of the commercial crane, and its configuration is shown in Figure 11. The parameter values of the small crane in Figure 11 are shown in Table 3. To confirm the validity of the small crane and the commercial crane, the dynamics introduced in Section 2 was used. A comparison between the analytical and experimental results obtained by inputting a trapezoidal velocity trajectory with a cycloid curve

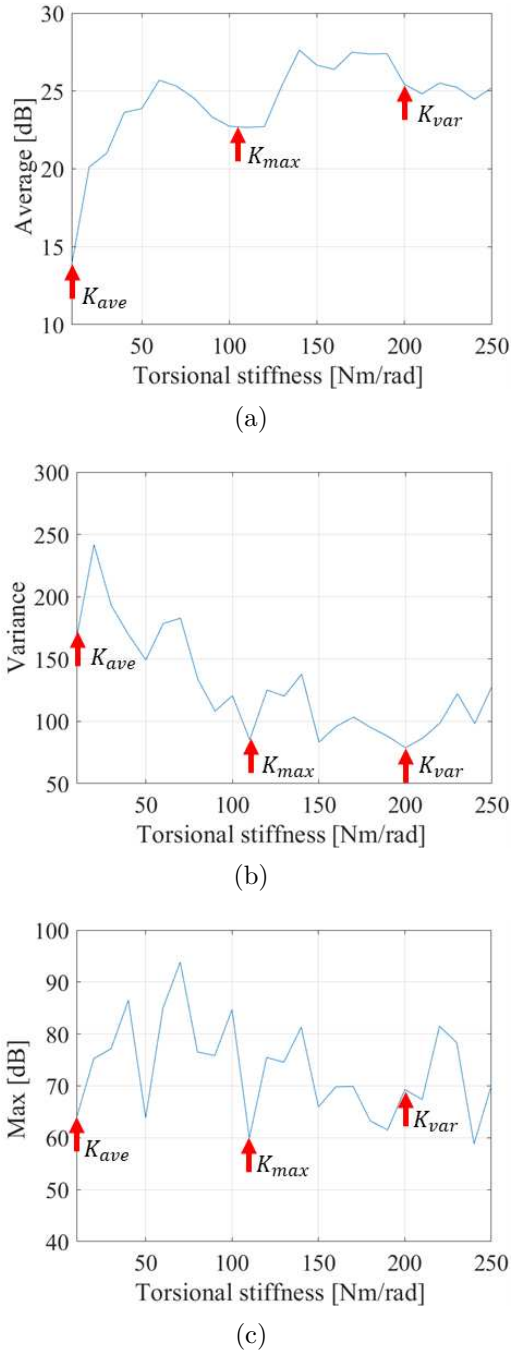

FIGURE 10. Selection of optimal torsional stiffness expected to provide the operational easiness: (a) Average, (b) variance and (c) maximum

whose terminal velocities and accelerations are 0 [rad/s^2] for acceleration and deceleration periods is shown in Figure 12. The experimental results are consistent with the simulation, and considering Figure 5, it is confirmed that the small crane can simulate the characteristics of the commercial crane.

For small cranes, the rope and mass of the load can be changed. The "spring mechanism" between the motor output shaft and the tower, whose details are given in the next section, can simulate tower torsion, and the torsional rigidity can be changed by replacing the spring. Figure 13 shows the real-time measurement system for small crane motion using eight motion-capture cameras installed on the safety fence. The small crane is driven

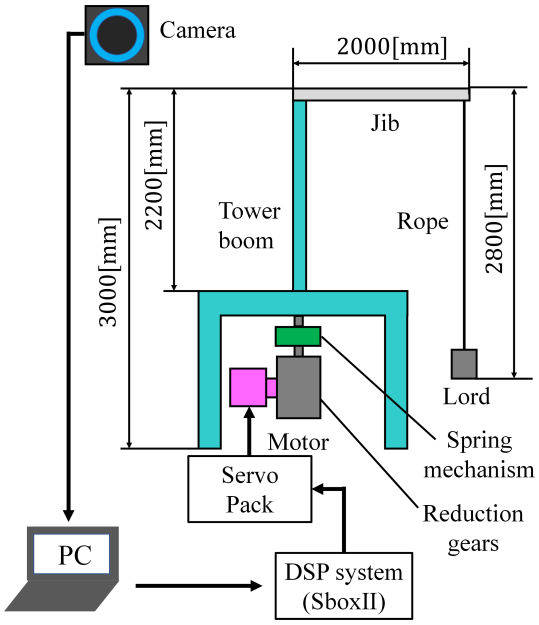

FIGURE 11. Experimental system

TABLE 3. Parameter values of the experimental crane in Figure 11

Item	Symbol [Unit]	Value
Tower length	L_t [m]	2.2
Jib length	L_j [m]	2.0
Rope length	l [m]	1.5, 2.8
Load mass	m [kg]	2.0, 3.0
Jib mass	m_j [kg]	3.2
Tower mass	m_t [kg]	36.0
Moment of inertia about x-axis (Tower and Jib)	I_x [kg m^2]	54.95
Moment of inertia about z-axis (Tower and Jib)	I_z [kg m^2]	2.19

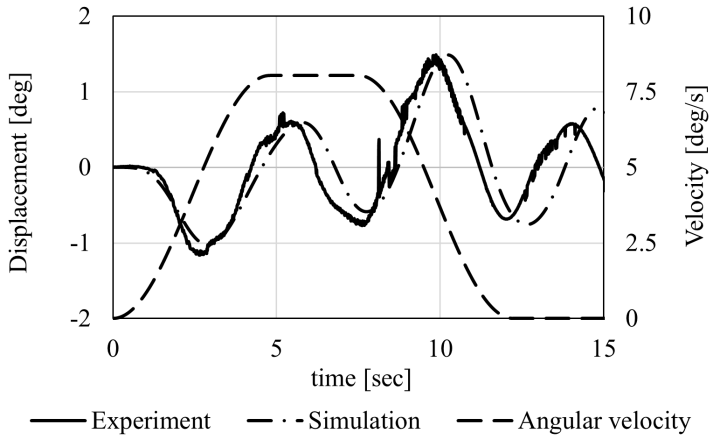

FIGURE 12. Comparative simulation results of commercial and experimental cranes

FIGURE 13. Motion capture camera placement

by a DSP (Digital Signal Processor) system that sends a velocity command voltage to the servo driver based on a pre-defined crane's angular velocity profile or lever operation.

4.2. **Spring mechanism.** In this study, a spring mechanism was installed between the servo motor and the tower to simulate the tower torsion in the commercial crane (see Figure 14). The approximate torsional stiffness of this mechanism was calculated as follows.

$$K \cong K_s l_s^2 \tag{8}$$

where notations are given in Table 4. Experimental verification was conducted under the following three conditions based on the torsional stiffness examined in Section 3: $K = 10$ [Nm/rad], 110 [Nm/rad], and 200 [Nm/rad].

FIGURE 14. Spring mechanism installed between the tower and its drive motor

TABLE 4. Parameter values of the selected springs

Item	Symbol [Unit]	1	2	3
Distance between tower rotational axis and spring force affecting point	l_s [mm]		115	
Linear stiffness of the spring in Figure 14	K_s [N/mm]	0.8	8.3	15.1
Experimental torsional stiffness	K [Nm/rad]	10	110	200

5. Experiment.

5.1. **Experimental conditions.** The following two tasks were assigned to the operators: 1) to transfer the load in consideration of residual load-sway and 2) to stop the existing load-sway at the desired position, as described in the following subsections. The experimental conditions are shown in Table 5. The torsional stiffness, rope length, and mass of the suspended load were varied in the experiment, and measurements were taken five times for each condition. The mean and standard deviation of the task completion time and the required time for load-sway suppression, as well as the operator's subjective evaluation, were used to evaluate the operability of the cranes. To simulate the operator's view in the commercial crane, the operator operates the small crane using only the camera image shown in Figure 15.

TABLE 5. Experimental conditions

Item	Symbol [Unit]	Value
Torsional stiffness	K [Nm/rad]	10 110 200 ∞
Rope length	l [m]	1.5 2.8
Load mass	m [kg]	2.0 3.0

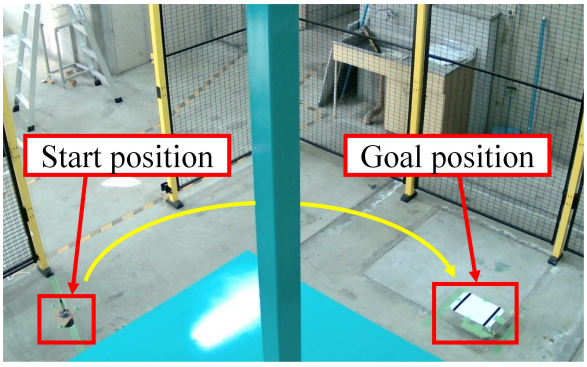

FIGURE 15. Operator's view and assigned task in the experiment

5.2. **Experiments of load transfer.** The operability of the cranes in transferring loads was compared. An experiment was conducted with four students assuming unskilled operators to investigate the effect of the spring stiffness obtained in the calculation described in Section 3 on the operability of cranes. In addition to the three spring stiffnesses, a condition assuming a rigid body ($K = \infty$) that drives the tower directly from the servomotor without a spring (Figure 14) is considered. As shown in Figure 15, the operator was asked to rotate the tower to move a load to a white area at a goal position 75 [deg] away. The operator was asked to move the load between the two black lines (distance between the lines: 100 [mm]) at the goal as quickly as possible and to stop the load in place. Each of the four subjects underwent operations five times under each experimental condition. The transfer operation times for all subjects are shown in Figure 16. The results of a t-test performed to determine whether there is a statistical difference for each average of the

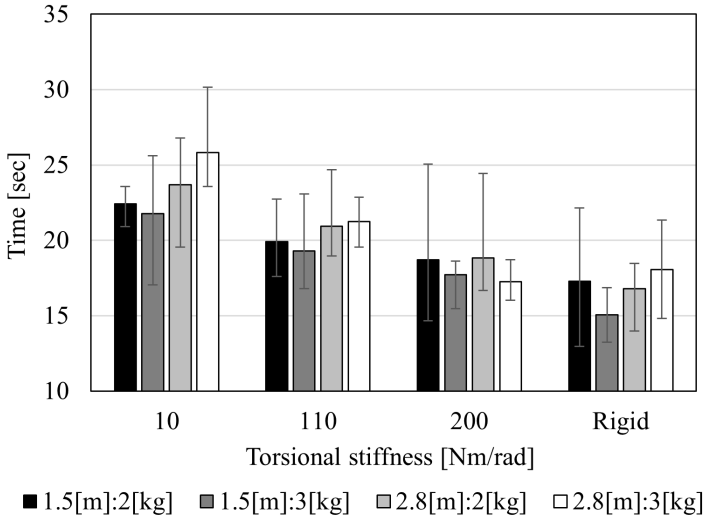

FIGURE 16. Experimental results of load transfer

TABLE 6. p-values in t-test of load transfer time

Torsional stiffness [Nm/rad]	10	110	200	Rigid
10	–	1.88×10^{-5}	2.9×10^{-12}	4.96×10^{-16}
110	–	–	1.43×10^{-4}	3.05×10^{-8}
200	–	–	–	0.0313
Rigid	–	–	–	–

load transfer time are shown in Table 6. The number of samples was 80, which is sufficient for t-test [33]. The p-values for the conditions in each row against each column are also shown in Table 6. Torsional stiffness was statistically significant at p-value < 0.05 for all combinations of $K = 10$, 110, and 200 [Nm/rad], as well as the rigid body (Table 6). The higher the torsional stiffness of the tower, the shorter the load transfer time (Table 6 and Figure 16).

Figure 17 shows the average and standard deviation of the residual load-sway of the four subjects. The results of a t-test for each average of the load-sway after load transfer are shown in Table 7. The residual load-sway was the smallest when the torsional stiffness was 10 [Nm/rad], which is considered easier to control than others. This is because elasticity absorbs small load-sway. The highest load-sway angles and standard deviations were observed in the rigid body condition. Additionally, the residual load-sway is reduced for longer rope lengths overall.

5.3. **Experiments on suspension of load-sway.** As shown in Figure 18, initial displacement (280 [mm] for $l = 2.8$ [m] and 150 [mm] for $l = 1.5$ [m]) was applied in the tangential direction to the tower rotational circle to produce a load-sway of 0.1 [rad], and operators were asked to stop load-sway operation. The time until the load was visually stopped was measured from the camera image in Figure 15. Four subjects operated the crane five times for each condition in Table 5.

Figure 19 shows the average, maximum, and minimum time staken by the four subjects to complete the task. The results of t-tests to verify the statistical differences are shown in Table 8.

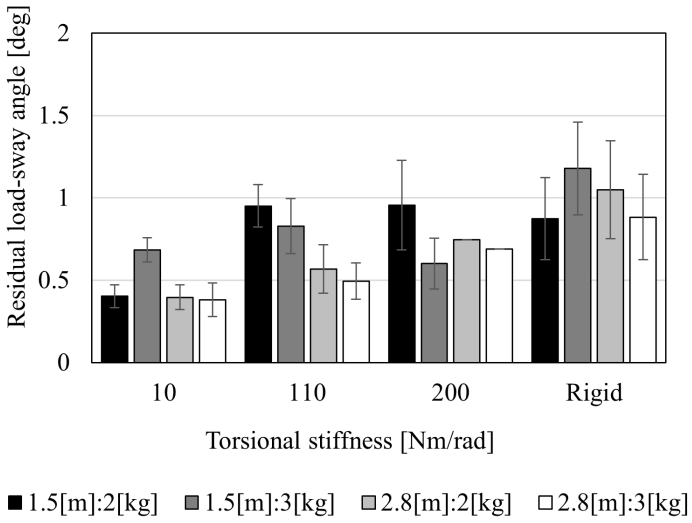

FIGURE 17. Residual load-sway of load transfer

TABLE 7. p-values in t-test of load-sway after load transfer

Torsional stiffness [Nm/rad]	10	110	200	Rigid
10	–	1.08×10^{-4}	8.95×10^{-6}	2.36×10^{-10}
110	–	–	0.589	0.0017
200	–	–	–	0.0099
Rigid	–	–	–	–

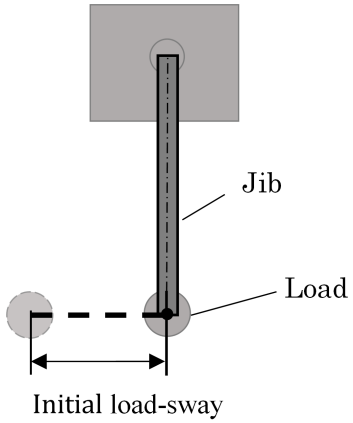

FIGURE 18. Initial load-sway for suppression experiment

Figure 19 and Table 8 show that the highest suppression time on average is statistically at 10 [Nm/rad]. There were no significant differences among others. Figure 20 shows the residual load-sway after load-sway suppression. The results of the t-tests used to confirm the statistical differences are shown in Table 9. The average residual load-sway is minimum at a torsional stiffness of 200 [Nm/rad]. At low torsional stiffness, active anti-sway control is difficult, resulting in a different trend than in the case of load transfer in Figure 17.

5.4. **Subjective operability evaluation by questionnaire.** After the work was completed, the subjects were asked to answer a usability questionnaire (5-point scale: best 5), and the results are shown in Figure 21. The following three survey items were used.

1) Transportability: Ease of transferring the load to the goal position

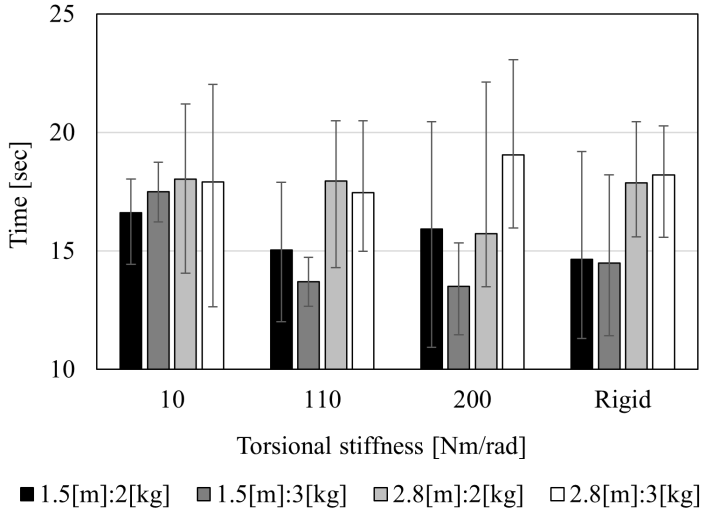

FIGURE 19. Experimental results of load-sway suppression time

TABLE 8. p-values in t-test of load-sway suppression time

Torsional stiffness [Nm/rad]	10	110	200	Rigid
10	–	0.037	0.041	0.077
110	–	–	0.986	0.722
200	–	–	–	0.738
Rigid	–	–	–	–

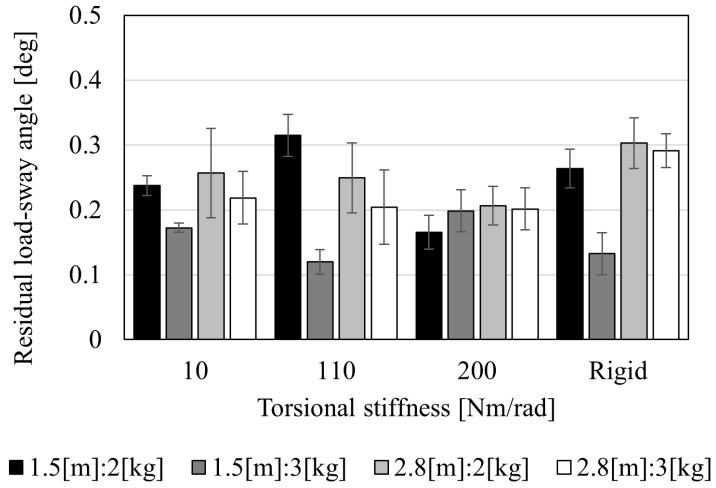

FIGURE 20. Residual load-sway after operation of load-sway suppression

TABLE 9. p-values in t-test of load-sway after operation of load-sway suppression

Torsional stiffness [Nm/rad]	10	110	200	Rigid
10	–	0.978	0.099	0.19
110	–	–	0.18	0.283
200	–	–	–	0.051
Rigid	–	–	–	–

2) Followability: Good tracking in response to the lever movement
3) Load-sway suppression: Ease to stop the load-sway by lever action

Figure 21(a) shows that the higher the torsional stiffness in the questionnaire, the higher the transfer, followability, and load-sway suppression properties. Figure 16 shows that higher stiffness enables faster for the goal position. Figure 21(b) shows that the rigid body has the highest value for load-sway suppression. A torsional stiffness of 200 [Nm/rad] is still rated higher in load-sway suppression, indicating that the higher the torsional stiffness, the better the operability. Considering the results in Figures 17, 20, and 21, a tower with some stiffness is easier to suppress the load-sway than a rigid case. When the jib is pulled by the load, the torsional stiffness of the tower acts as a damper against the load-sway. In the active load-sway suppression results in Figure 20, the highest stable load-sway suppression was observed at a torsional stiffness of 200 [Nm], providing the smallest variance of the second-order mode vibration gain (Figure 10(b)). Based on the verification results, we concluded that the tower torsional stiffness should be designed to reduce the variance and magnitude of the second-order mode gain.

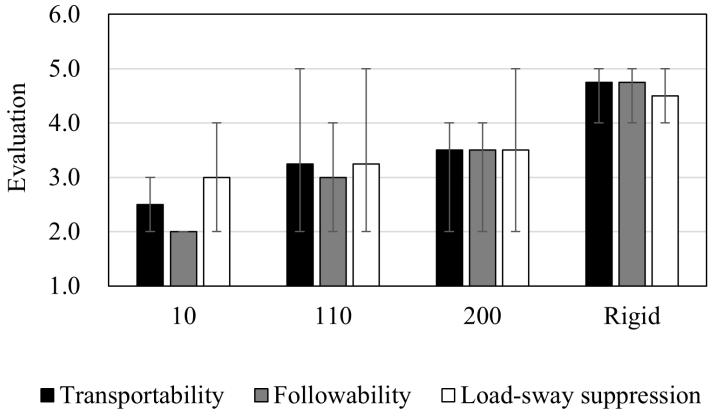

(a)

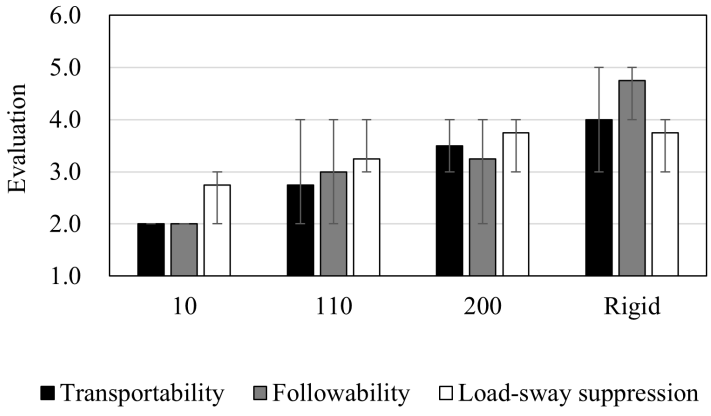

(b)

Figure 21. Results of questionnaire: (a) Load transfer and (b) load-sway suppression

6. **Conclusions.** An experimental system was designed to simulate the torsion of an actual tower crane. The optimal torsional stiffness of the tower was determined using simulation based on dynamic characteristics. Load transfer and load-sway suppression tests, and a questionnaire survey were conducted, which statistically demonstrated that torsional

stiffness can improve the operability of cranes by reducing not only the magnitude of the second-mode gain but also its variance. Future work includes the application of this second-order mode gain reduction method to the typical design with the finite element method for the truss structure. The effectiveness will be verified with the actual tower crane by simulation and experiment. In addition, the proposed approach can be applied to not only crane systems but also other mechanical systems that require the reduction of the second-order mode gain.

REFERENCES

[1] Y. Zheng, F. Zhao and Z. Wang, Fault diagnosis system of bridge crane equipment based on fault tree and Bayesian network, *The International Journal of Advanced Manufacturing Technology*, vol.105, pp.3605-3618, DOI: https://doi.org/10.1007/s00170-019-03793-0, 2019.

[2] B. He, W. Tang and J. Cao, Virtual prototyping-based multibody systems dynamics analysis of offshore crane, *SIAM J. Control and Optimization*, vol.75, pp.161-180, DOI: 10.1007/s00170-014-6137-4, 2014.

[3] A. Li and C. Liu, Lightweight design of a crane frame under stress and stiffness constraints using super element technique, *SAGE Advances in Mechanical Engineering*, vol.9, no.8, pp.1-15, DOI: https://doi.org/10.1177/1687814017716621, 2017.

[4] L. Li, L. Bai, G. Wei, N. Shi, N. Wang, M. Ye, H. Gu, X. Xu and J. Liu, Reliability based design optimization for the lattice boom of crawler crane, *Structures*, vol.29, pp.1111-1118, DOI: https://doi.org/10.1016/j.istruc.2020.12.024, 2021.

[5] R. Peek and N. Triantafyllidis, Worst shapes of imperfections for space trusses with many simultaneously buckling members, *International Journal of Solids and Structures*, vol.29, pp.2385-2402, DOI: https://doi.org/10.1016/0020-7683(92)90222-F, 1992.

[6] C. Zhou, Y. Shen and Z. Wang, Research on vibration suppression of transmission chain in wind power generation system with gear clearance based on internal model control, *International Journal of Innovative Computing, Information and Control*, vol.18, no.4, pp.1247-1263, DOI: https://doi.org/10.24507/ijicic.18.04.1247, 2022.

[7] H. Wu, D. Zhang and Q. Cheng, Analysis of transverse vibration of high-velocity elevator with variable-length hoisting system, *ICIC Express Letters, Part B: Applications*, vol.10, no.5, pp.379-386, DOI: https://doi.org/10.24507/icicelb.10.05.379, 2019.

[8] L. Rincon, Y. Kubota, G. Venture and Y. Tagawa, Inverse dynamic control via "simulation of feedback control" by artificial neural networks for a crane system, *Control Engineering Practice*, vol.94, 104203, DOI: 10.1016/j.conengprac.2019.104203, 2020.

[9] K. Matsui and H. Kajiwara, Feedforward control input generation method for a crane system with restrictions on drive system, *Mechanical Systems and Signal Processing*, vol.170, 108865, DOI: 10.1016/j.ymssp.2022.108865, 2022.

[10] H. Ouyang, X. Xu, T. Ganbat and G. Zhang, Nonlinear adaptive based swing reduction control for rotary cranes with double pendulum effect considering uncertain parameters and external disturbances, *Automation in Construction*, vol.126, 103668, DOI: https://doi.org/10.1016/j.autcon.2021.103668, 2021.

[11] S. Hu, Y. Fang and H. Guo, A practicality and safety-oriented approach for path planning in crane lifts, *Automation in Construction*, vol.127, 103695, DOI: https://doi.org/10.1016/j.autcon.2021.103695, 2021.

[12] S. Messineo, F. Celani and O. Egeland, Crane feedback control in offshore moonpool operations, *Control Engineering Practice*, vol.16, pp.356-364, DOI: 10.1016/j.conengprac.05.003, 2008.

[13] I. Mizumoto, T. Chen, S. Ohdaira, M. Kumon and Z. Iwai, Adaptive output feedback control of general MIMO systems using multirate sampling and its application to a cart-crane system, *Automatica*, vol.43, pp.2077-2085, DOI: 10.1016/j.automatica.2007.04.017, 2007.

[14] S. Chwastek, Optimization of crane mechanisms to reduce vibration, *Automation in Construction*, vol.119, 103335, DOI: https://doi.org/10.1016/j.autcon.2020.103335, 2020.

[15] Z. Li, X. Ma and Y. Li, Nonlinear partially saturated control of a double pendulum offshore crane based on fractional-order disturbance observer, *Automation in Construction*, vol.137, 104212, DOI: https://doi.org/10.1016/j.autcon.2022.104212, 2022.

[16] M. Zhang, Y. Zhang, B. Ji, C. Ma and X. Cheng, Adaptive sway reduction for tower crane systems with varying cable length, *Automation in Construction*, vol.119, 103342, DOI: https://doi.org/10.1016/j.autcon.2020.103342, 2020.

[17] R. Mar, A. Goyal, V. Nguyen, T. Yang and W. Singhose, Combined input shaping and feedback control for double-pendulum systems, *Mechanical Systems and Signal Processing*, vol.85, pp.267-277, DOI: 10.1016/j.ymssp.2016.08.012, 2017.

[18] K. Terashima, Y. Shen and K. Yano, Modeling and optimal control of a rotary crane using the straight transfer transformation method, *Control Engineering Practice*, vol.15, pp.1179-1192, DOI: 10.1016/j.conengprac.2007.02.008, 2007.

[19] S. Sano, H. Ouyang, H. Yamashita and N. Uchiyama, LMI approach to robust control of rotary cranes under load sway frequency variance, *Journal of System Design and Dynamics*, vol.5, pp.1402-1417, DOI: 10.1299/jsdd.5.1402, 2011.

[20] J. Neupert, W. Arnold, K. Schneider and O. Sawodny, Tracking and anti-sway control for boom cranes, *Control Engineering Practice*, vol.18, pp.31-44, DOI: 10.1016/j.conengprac.2009.08.003, 2010.

[21] H. Takahashi, A. Farrage, K. Teraushi, S. Sasai, H. Sakurai, M. Okubo and N. Uchiyama, Sensor-less and time-optimal control for load-sway and boom-twist suppression using boom horizontal motion of large cranes, *Automation in Construction*, vol.134, 104086, DOI: https://doi.org/10.1016/j.autcon.2021.104086, 2022.

[22] N. Sun, Y. Fu, T. Yang, J. Zhang, Y. Fang and X. Xin, Nonlinear motion control of complicated dual rotary crane systems without velocity feedback, *IEEE Transactions on Automation Science and Engineering*, vol.17, pp.1017-1029, DOI: 10.1109/TASE.2019.2961258, 2020.

[23] H. Ouyang, X. Xu and G. Zhang, Tracking and load sway reduction for double-pendulum rotary cranes using adaptive nonlinear control approach, *International Journal of Robust and Nonlinear Control*, vol.30, pp.1872-1885, DOI: https://doi.org/10.1002/rnc.4854, 2020.

[24] H. Ouyang, X. Xu and G. Zhang, Energy-shaping-based nonlinear controller design for rotary cranes with double-pendulum effect considering actuator saturation, *Automation in Construction*, vol.111, 103054, DOI: https://doi.org/10.1016/j.autcon.2019.103054, 2020.

[25] N. Uchiyama, H. Ouyang and S. Sano, Simple rotary crane dynamics modeling and open-loop control for residual load sway suppression by only horizontal boom motion, *Mechatronics*, vol.23, pp.1223-1236, DOI: https://doi.org/10.1016/j.mechatronics.2013.09.001, 2013.

[26] Kobelco Construction Machinery Co., Ltd., *Crawler Crane*, https://www.kobelco-kenki.co.jp/products/crawler_cranes/, Accessed on Oct. 15, 2022.

[27] Libeherr, *Hydro-Crane-Club*, http://www.hydro-crane.com/liebherr/, Accessed on Oct. 15, 2022.

[28] ZOOMLION, *Mobile Crane*, https://en.zoomlion.com/channel/9b442fdb031345b59cb3ca24da55b137.html?type=3&isChannel=0&isSelect=1&typeId=013dd785a8644e48858d6243eecb6b99, Accessed on Oct. 15, 2022.

[29] C. O. Azeloglu, S. Ozen, A. Edincliler and H. Kenan, Natural frequency analysis of lattice boom crane theoretically and experimentally, *International Journal of Steel Structures*, vol.17, pp.757-762, DOI: 10.1007/s13296-017-6029-1, 2017.

[30] X. Kong, Z. Qi and G. Wang, Elastic instability analysis for slender lattice-boom structures of crawler cranes, *Journal of Constructional Steel Research*, vol.115, pp.206-222, DOI: 10.1016/j.jcsr.2015.07.027, 2015.

[31] H. Araya, M. Kakuzen, H. Kinugawa and T. Arai, Level luffing control system for crawler cranes, *Automation in Construction*, vol.13, pp.689-697, DOI: 10.1016/j.autcon.2004.04.011, 2004.

[32] A. A. Elbadawy and M. M. G. Shehata, Anti-sway control of marine cranes under the disturbance of a parallel manipulator, *International Conference on Engineering and Technology (ICET)*, vol.85, pp.415-434, DOI: 10.1109/ICEngTechnol.2014.7016748, 2015.

[33] J. N. Rouder, P. L. Speckman, D. Sun and R. D. Morey, Bayesian t tests for accepting and rejecting the null hypothesis, *Psychonomic Bulletin & Review*, vol.16, pp.225-237, DOI: https://doi.org/10.3758/PBR.16.2.225a, 2009.

Author Biography

Hideki Takahashi received the associate B.E. degree from Kochi National College of Technology, Kochi, Japan, in 2013, the B.E. and M.E. degrees from Nagaoka University of Technology, Niigata, in 2015 and 2017, respectively. He has been with Kobelco Construction Machinery Co., Ltd. since 2017, joined Toyohashi University of Technology as a researcher in 2019, enrolled in the doctoral program of Toyohashi University of Technology in the same year, and expected to complete it in 2023. He is interested in design and control of industrial crane systems.

Fumiya Tsukahara received the associate B.E. degree from Gifu National College of Technology, Gifu, Japan, in 2016, the B.E. and M.E. degrees from Toyohashi University of Technology, Aichi, in 2018 and 2021, respectively. He has been with Meitec Corporation since 2021. He is interested in design and control of mechanical systems.

Kenichi Terauchi received the B.E. and M.E. degrees from Kyoto Institute Technology, in 1992 and 1994, respectively. He joined Kobelco Construction Machinery Co., Ltd. in 1994. He has been a visiting professor at Toyohashi University of Technology since 2018. He is interested in design and control of industrial crane systems.

Shintaro Sasai received the B.E. degree from Hiroshima Institute of Technology in 1997. He has been with Kobelco Construction Machinery Co., Ltd. since 2004. He is interested in design and control of industrial crane systems.

Hitoshi Sakurai received the B.E. and M.E. degrees from University of Hyogo, Hyogo, Japan, in 2006 and 2008, respectively. He has been with Kobelco Construction Machinery Co., Ltd. since 2008. He is interested in design and control of industrial crane systems.

Masaki Okubo received the B.E. and M.E. degrees from University of Hyogo, Hyogo, Japan, in 2014 and 2016, respectively. He has been with Kobelco Construction Machinery Co., Ltd. since 2016. He is interested in design and control of industrial crane systems.

Naoki Uchiyama received the associate B.E. degree from the Numazu National College of Technology, Shizuoka, Japan, in 1988, the B.E. and M.E. degrees from Shizuoka University, Shizuoka, in 1990 and 1992, respectively, and the Ph.D. degree in Mechanical Engineering from Tokyo Metropolitan University, Tokyo, Japan, in 1995. Since 1995, he has been with the Department of Mechanical Engineering, Toyohashi University of Technology, Japan, where he is currently a professor. He was a visiting scholar of the University of California, Davis from 2001 to 2002, and a visiting professor of Universiti Teknologi MARA, Malaysia and the University of Stuttgart, Germany in 2022. His research interests include optimization, control and mechatronics.